Granular Matter (2007) 9:309–321
DOI 10.1007/s10035-007-0046-2

A physically based approach to granular media mechanics: grain-scale experiments, initial results and implications to numerical modeling

David M. Cole · John F. Peters

Received: 30 September 2005 / Published online: 18 July 2007

Abstract It is generally appreciated that the mechanical behavior of granular media depends fundamentally on the interaction of the constituent particles, and that the validity of numerical models of granular media would be greatly improved with knowledge of the grain-scale mechanics. However, most supporting experimental work has been conducted on highly idealized materials, and a limited amount of information exists on grain-scale force–displacement relationships for naturally occurring materials. To address this shortcoming, we are conducting a program that integrates laboratory experiments on grains of naturally occurring aggregate with the discrete element modeling method, with the goal of relating the grain-scale physical and mechanical properties of granular media to bulk behavior. The paper describes the equipment and methods that have been developed to conduct close-loop controlled, grain-scale experiments under monotonic and cyclic loading conditions, and presents results from an initial set of experiments on unbonded grains. The implications of the grain-scale results to the discrete element model are discussed. Discussions center on the applicability of a physically based approach to the mechanics of granular media in general. In light of future exploration missions and the resulting need to predict the mechanical properties of lunar and planetary regoliths, the paper examines the potential usefulness of our physically based approach to the problem of predicting the behavior of the types of materials found in those environments.

Keywords Micromechanics · Contact mechanics · Experiments · Friction · Geologic materials

D. M. Cole (✉)
Cold Regions Research and Engineering Laboratory,
Engineer Research and Development Center
U.S. Army Corps of Engineers, 72 Lyme Rd.,
Hanover, NH 03755, USA
e-mail: David.M.Cole@erdc.usace.army.mil

J. F. Peters
Geotechnical and Structures Laboratory,
Engineer Research and Development Center
U.S. Army Corps of Engineers, Vicksburg, MS, USA

1 Introduction

Current numerical models can compute the mechanical behavior of granular media based on the interaction of a large number of discrete components. These models have found applications in industrial problems, civil engineering, sea ice dynamics and granular media research. When given the proper micromechanical basis, such computer simulations improve our understanding of how granular media behave on a very fundamental level, and thus have great value as predictive tools to improve material design methods, and to support the development of constitutive relationships for continuum-based analysis. Furthermore, this approach is particularly attractive for work on cohesionless and large-grained media that are difficult to sample, and can be employed to conduct virtual experiments to examine behavior under conditions that are difficult to reproduce in the laboratory. For example, experiments involving shear tractions at specimen boundaries (e.g., [1]) are very difficult to conduct and are typically restricted to research-level experiments on uniform sand or clay. Such situations could be readily examined numerically with models that have an adequate physical basis.

In addition to examining terrestrial materials, an intriguing application for physically based granular media simulation is the prediction of the mechanical properties of lunar and planetary regoliths, for which in-situ testing is difficult and return sampling for terrestrial testing is extremely expensive.

An ultimate goal of the present effort is to employ experimentally measured micromechanical properties and the geometry of the constituent particles in the numerical simulation of the mechanical behavior of granular media. However, a number of technical challenges must be overcome in both the numerical models and the experimental methodologies before this goal can be realized. Improvements are required in the computing software to deal with realistic particle size gradations and shapes. Numerical time integration schemes pose practical limits to the particle mass and stiffness that can be used to model interactions at contacts. Yet, both algorithms and hardware are advancing quickly and it is reasonable to expect that numerical modeling capabilities will soon rise to a level acceptable for practical purposes.

On the other hand, methodologies for measuring the grain-scale mechanical properties of naturally occurring materials at the scales of interest here (e.g., on the order of 10^{-3} m and larger) have not advanced in step with numerical procedures. There has been progress with experiments at a much finer scale, however. The equipment used in atomic force microscopy (AFM) has been successfully adapted to perform mechanical properties and friction experiments on the micro- and nano-scales [13,15]. This approach is capable of resolving forces on the scale of nN, with spatial resolution on the order of nm, and can resolve periodicity in sliding friction on the scale of atomic spacing. Although such work has direct application in the area of nanotribology (e.g., [2]), it examines behavior at a physical scale that is several orders of magnitude smaller than the scale of interest to many engineering problems.

Experimental methods have been developed to observe particle motion in three-dimensional grain assemblies, and progress has been made in identifying specific micro-scale deformation mechanisms. However, it is generally necessary to assume the underlying particle interaction laws. Although the resulting simulations can produce reasonable engineering behavior, there is no guarantee of the uniqueness of the assumed laws or that they adequately capture the details of the underlying physical processes. Consequently, the intent of our micro-scale experiments is to isolate and quantify the grain-scale interactions that underlie bulk behavior. The resulting particle interaction laws will provide a physical, rather than phenomenological basis for the numerical simulations. This, in turn, will greatly enhance the usefulness and reliability of the simulations.

This paper describes our initial efforts to develop experimental procedures to explore particle contact mechanics in support of discrete model development for research on granular media, and presents the results of our initial experiments on unbonded grain pairs subjected to cyclic and monotically increasing normal contact loading. The micro-scale behavior is examined in the context of the discrete element modeling framework and the implications of the observed behavior on the macroscopic response of the material is considered.

2 Micromechanical observations

The bulk of laboratory experiments conducted in conjunction with discrete element model development have frequently employed idealized materials, with a focus on observing particle motion under gravitational or forced loading, and/or stress transmission through assemblies of particles. Such studies have served to verify the mechanical behavior (e.g., [20]) and microstructural evolution [19], predicted by numerical models. Such experiments provide critical insight regarding stress transmission and the relative motion of particles (normal, shear, rolling), and facilitate a mechanistic approach to granular media mechanics [23]. These efforts have made it possible to identify and simulate, for example, the development of force chains [16,21], and demonstrated the role of processes such as particle rolling and normal contact in granular media. Although some of the studies conducted in support of numerical model development have addressed the influence of the actual physical properties of the particles (e.g., [12]), it appears that incorporation of detailed descriptions of the actual contact mechanics has generally been considered to be too burdensome computationally.

By identifying the important micromechanical deformation mechanisms, previous studies have made critical contributions to our understanding of the micromechanics of granular media mechanics. However, when attempting to extend the numerical models to applications involving naturally occurring (e.g., highly variable, rather than ideal) materials, it is necessary to employ contact laws that reflect actual material behavior. The static and dynamic sliding friction of a number of minerals has been examined [14] in laboratory experiments. In those experiments, mineral type, lubrication and surface roughness were found to influence sliding friction, and stick–slip behavior was frequently observed. Despite the equipment limitations of the day, those results provide a clear indication that the bulk properties and microscopic surface characteristics of the material exert an influence on the particle interaction mechanics. As far as naturally occurring materials are concerned, deformation modes other than pure sliding have apparently not been well investigated and the present laboratory effort is motivated by the need for more complete experimental information to support the development of realistic laws for the particle-scale mechanics.

With regard to the experimental methodology applied in the present effort, it is noted that the combination of monotonic and cyclic loading methods has been used for some time in the development of mechanistic models of various types of ice and ice–soil mixtures [3–6]. That work used the

cyclic loading response coupled with a dislocation mechanics analysis to query the state of the defect population of a specimen as a function of its stress state and loading history. The cyclic response is particularly informative in this regard because it readily provides information on both the elastic and inelastic deformation of the material, and can thus be used to decompose the macroscopic load–deformation response into its components. Although the underlying mechanisms of deformation are completely different in the case of grain interactions, this approach can readily be applied to support the development of mechanistic models applicable to the particle scale.

3 Discrete element method

The discrete element method (DEM) of Cundall and Strack [7] treats the granular medium as a collection of interacting discrete objects. Each object moves in accordance with Newton's laws of motion in response to the total force that results from contact with other particles and body forces such as gravity and inertia (Fig. 1). The motion of each particle is described by a velocity ($\mathbf{v}$) and rotation ($\boldsymbol{\omega}$) at the center of the particle. The contact forces between particle pairs are a result of the relative motion at the point of contact, as defined by $\mathbf{v}_A^c$ and $\mathbf{v}_B^c$, which result from a combination of relative translation ($\mathbf{v}_B - \mathbf{v}_A$) and relative rotation ($\boldsymbol{\omega}_B - \boldsymbol{\omega}_A$). The relationship between the contact motions and resisting forces define the micro-scale properties of the medium. The constitutive response of the material at the macro-scale is an emergent property that is the result of the collective response of the aggregate, and depends on the micro-scale properties, the stochastic nature of the particle arrangement and boundary conditions.

The contact motions and their conjugate forces are decomposed into normal and shear components as shown in Fig. 2. The forces acting at a contact between two particles consist of three components conjugate to the three modes of relative

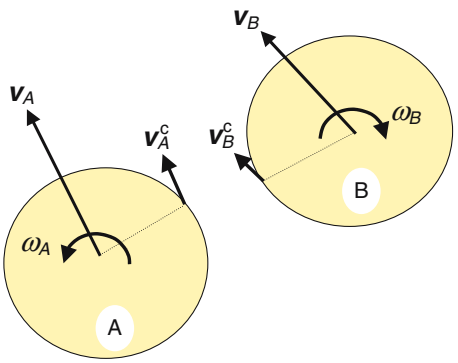

Fig. 1 Kinematic variables for two contacting particles

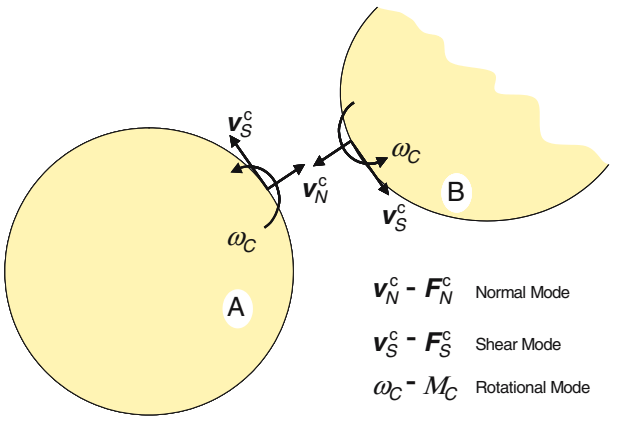

Fig. 2 Relative contact motion and their conjugate force pairs

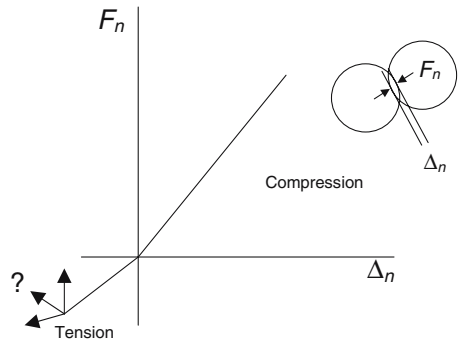

Fig. 3 Idealized force law for normal contacts

motion. The normal mode consists of motions ($\mathbf{v}_N^c$) directed along the normal direction of the contact and are resisted by either compressive or tensile forces ($\mathbf{f}_N^c$) (Fig. 3). In DEM these forces are often assumed to be modeled as a simple linear spring that relates $\mathbf{f}_N^c$ to the total penetration Δ_n. However, in many codes the contact is modeled after Hertz contact theory for contacting spheres in which the force is proportional to $\Delta_n^{3/2}$. While the Hertz theory for elastic interaction for spheres has been verified, its applicability to actual soil particles is not as well known. First, the contact response might not be elastic, due to degradation or damage at the point of contact. The degradation of contact asperities gives a stiffening effect that can mask the elastic behavior of the Hertz contact. Further, actual particles are not spherical. Finally, at the particle scale, the material behavior is typically not isotropic but is determined by the character of the mineral from which it is formed. Therefore, one aim of the present investigation is to determine the importance of modeling the elastic contact behavior precisely in natural soil particles.

Figure 4 depicts the shear or tangential mode of contact deformation. The response to the motion is initially elastic followed by slipping once the Coulomb limit criterion is met. A similar response is modeled for rolling resistance which is assumed to be proportional to the magnitude of the normal

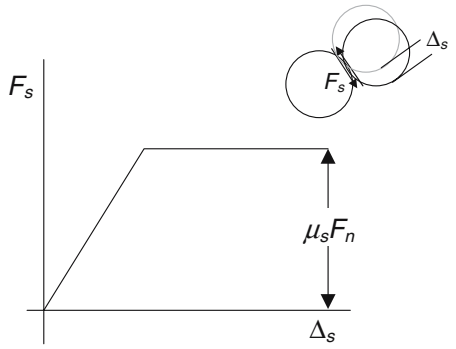

Fig. 4 Idealized contact law for shear

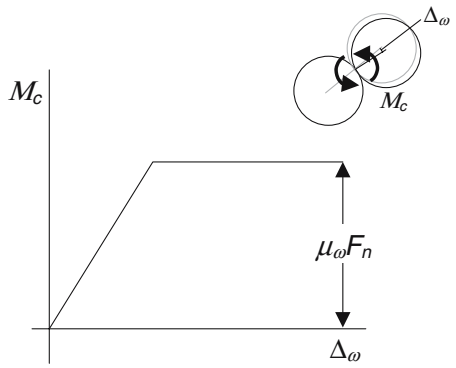

Fig. 5 Idealized contact law for contact moment

force (see Fig. 5). Not shown is the torsional mode in which the relative rotation vector is aligned with the normal axis. The torsional mode is of greatest interest in bonded materials.

In bonded media, the tensile force is not zero but is limited by a bonding strength. The bonding strength is more complicated than the conventional frictional contact law used in DEM because the limit load for each mode depends on the combination of loads present [8,9,22]. Figure 6 depicts conceptually how the interaction of loads affects the bond strength. The delineation of the limit surface is the organizing principle for future efforts in our research program. A critical question in bonded media is the loss of force once the tensile limit is exceeded (Fig. 3). As bonding is lost, a brittle macro-scale response is created that is difficult to understand from macro-scale observations. For example, preliminary computations by us show that the relative stiffness of the bonded contact in the three modes, as well as the bonding strength, can influence the macro-scale failure mode. Sorting out such interactions is greatly simplified through a combination of macro-scale observations and DEM based on independent particle-scale measurements.

Not shown in Figs. 3, 4 and 5 is the response to load reversals. The contact force–displacement laws must contain damping for realistic simulation. The damping is generally incorporated either as a viscous damping or a hysteretic (rate-independent) curve calibrated to reproduce a reasonable

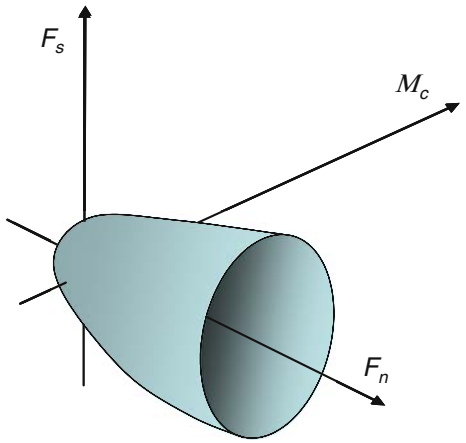

Fig. 6 Shear-normal, moment-normal, and shear-moment limit surfaces (conceptual)

coefficient of restitution. Where the micro-scale calibration can be compared with macro-scale results, realistic behavior can be obtained—particularly in the case of cohesionless materials. Where macro-scale computations are not available or there are limited micro-scale data to guide the calibration, an empirical approach is typically adopted. For example, energy dissipation is quantified by assuming a micro-scale law that has no specific physical basis, and the damping coefficient is assigned empirically to obtain realistic macro-scale behavior. Computations strongly suggest that even though slip (e.g., shear deformation) would appear to be the principal macro-scale mechanism for dissipation, the micro-scale mechanism that actually dissipates the energy is inter-particle motions in the normal mode.

The preceding paragraph illustrates the need for experiments that explicitly quantify the damping associated with specific mechanisms of particle interaction. As demonstrated in the following sections, the approach adopted in our work involves in part the explicit determination of inter-particle damping with cyclic loading experiments. Our initial experiments focus on the normal contact mode of unbonded contacts, and extension to other contact modes (shear, rolling) with and without bonding are planned.

4 Experimental procedures

Figure 7 shows a photograph of the experimental system configured for uniaxial loading of grain pairs. This is a computer-controlled, electro-mechanical system that employs a voice coil actuator to apply loads, a non-contacting laser sensor to measure the relative deformation of the specimen mounting pins, and a bonded strain gauge load cell to monitor the axial force applied to the specimen and provide a feedback signal to the control system. A graphical user interface (GUI) was developed to set the test parameters (load path, amplitude and frequency for cyclic loading experiments, data

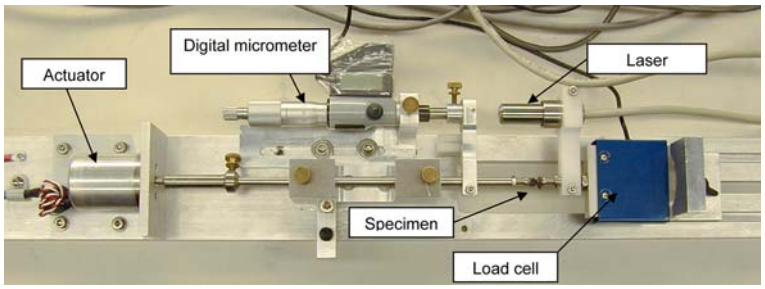

Fig. 7 Photograph of the experimental system

acquisition rate, etc.) and perform the closed-loop control functions. The system also employs a digital micrometer for positioning and calibration of the laser sensor. The experiments reported below employed a load cell with a 25 N capacity, and laser sensors that provided a ten VDC output for nominal ranges of 300 or 100 μm. The resolution of the displacement measuring system is on the order of 100 nm.

For the experiments presented below, the system was operated in closed-loop load control (e.g., the axial load on the grain pair was the controlled variable), and three load paths were employed in the experiments. Under the ramp loading, the normal force on the grain pair increased linearly at a specified rate to a maximum value. With the haversine waveform, the normal force cycled between a nominal no-load contact and a maximum value at a specified frequency (typically between 10^{-3} and 5 Hz). The third waveform consisted of a sinusoidally varying load of a given amplitude and frequency superimposed on a compressive background force. An analysis of the cyclic component of the latter waveform allows us to examine stiffness and damping as a function of the background force and is intended to provide insight into confining pressure effects.

The load and deformation readings are digitized and recorded as a function of time. The post-test analysis smoothes the raw data and calculates quantities such as the actual loading and deformation rates, frequency and hysteresis loop area when applicable, peak load, internal friction and the average slope during a cycle of loading. The smoothing is done by conducting a series of piece-wise regression fits to the raw data, rather than applying a running average (which can cause a phase shift in time-based data) and the methodology is fully described in Cole and Durell [6]. With regard to the analysis of the cyclic loading response, the slopes reported below are determined from the zero-to-peak load and deformation values of the load–deformation curves. The frictional loss that occurs during cyclic loading of materials in general is frequently characterized by the internal friction (tan ϕ) are determined from [18]:

$$\tan\phi = \frac{\Delta W/W}{2\pi}. \tag{1}$$

Where ΔW is the hysteresis loop area, and W is the peak stain energy during a load cycle. Equation (1) is particularly useful when the response shows a measurable hysteresis loop area but the phase lag angle ϕ is too small to measure directly. Strictly speaking, Eq. (1) applies to sinusoidal (e.g., alternating tension/compression) loading, for which the peak load occurs at the quarter-cycle point. It also presupposes that the elastic modulus is constant through the entire loading cycle. In principle, Eq. (1) can be applied to haversine loading by analyzing it as a sine wave oscillating about the mean force. This treatment can provide reasonable values of tan ϕ when the peak-to-peak value of the cyclic force is sufficiently low that the curvature of the force–displacement relationship is inconsequential. However, that calculation can produce inappropriately high values of internal friction for the case of Hertzian behavior. The problem arises because of the increase in the slope of the force–displacement relationship with force that is characteristic of Hertzian behavior. This has the effect of decreasing the value determined for the stored strain energy per cycle (W) in the above expression, which in turn leads to a high value of tan ϕ.

When the curvature of the force–displacement relationship cannot be ignored, it is possible to derive Eq. (1) using a haversine waveform, in which the peak stored strain energy per cycle occurs at the mid-point of the cycle. This leads to the following expression:

$$\tan\phi_{\text{haversine}} = \frac{\Delta W/W}{\pi} \tag{2}$$

in which W is now the area under the load–deformation curve from the start of loading up to the peak load which occurs midway through the cycle. In the internal friction plot presented below, the internal friction was calculated from Eq. (2) for haversine loading that begins and ends at a nominally zero force.

Finally, note that this definition of internal friction is not synonymous with the angle of internal friction used in geotechnical analysis. Rather, it a measure of the energy dissipated by friction or micro-scale damage within the material on each side of the contact. This measure of loss is also to be distinguished from Coulombic friction created by tangential sliding of the contact. As specific deformation mechanisms of

granular media are investigated experimentally, and the damping associated with each is quantified, it will be important to specify the deformation mechanism to which an internal friction value applies (e.g., ϕ_{normal} and $\phi_{\text{tangential}}$).

5 Specimens and methodology

Two types of material were examined in our initial experiments: a recently processed (e.g., unweathered) gneiss—representative of relatively hard rock behavior and a randomly selected pair of grains of weathered, local (New Hampshire) gravel (see Fig. 8). The crushed gneiss was provided by a colleague (Prof. Ivar Horvli of the Norwegian University of Science and Technology), and is being subjected to an extensive series of laboratory triaxial experiments in a separate research program. Because the aggregate was somewhat large for our purposes, representative pieces were broken up and a variety of sizes and shapes of the resulting fragments were selected for our experiments. The grains were bonded to threaded stainless steel pins with epoxy. Care was taken to assure that the contact points were from the original surface of the grains. Scaled digital micrographs of the grains were obtained before and after testing. The profile of each grain was digitized from the micrographs and the radius of curvature of the contact point was determined as described in the following section.

Our initial observations on the gneiss indicated that the most stable and reproducible configuration was a relatively flat grain paired with a relatively pointed grain (see Fig. 8). It was important to center the point of contact between the two grains on the axis of loading. We note that the method of producing these grains leads to irregular shapes and sizes, making it difficult to mount them accurately, and the development of more precise mounting methods is a matter of on-going interest. The weathered aggregate, on the other hand, had more regular shapes and smooth, well-rounded surfaces. The size and shape of these grains made them relatively easy to center on the loading pins.

We note that microfracturing and/or frictional sliding was audible in the initial loading cycles when the higher force levels were applied to certain of the gneiss grains. However, since the focus of the present experiments was to quantify the intrinsic interaction of the grains, the data presented below do not include tests that produced any audible reports during loading, nor was there any visible evidence of damage to the grains used to generate the reported data. The initial effort described below focused on the development of the experimental equipment and methodology and our on-going work will produce a more detailed characterization of the test material.

6 Radius of curvature determination

Analytical treatments of contact mechanics depend critically on the radius of curvature of the objects in contact. Manufactured or processed materials can be machined and brought to an arbitrarily smooth finish such that the macroscopically observed curvature is applicable at the point of contact. As described in the following section, we have conducted experiments on processed materials with relatively smooth surfaces and a well-defined radius of curvature, and those results are in close agreement with elastic contact behavior. On the other

Fig. 8 Micrograph of a grain pair of crushed gneiss used in the experiments

hand, there is probably not a simple relationship between the radius of curvature and the force–displacement behavior of a contact in naturally occurring granular materials as a consequence of roughness and inelastic deformation at the contact. For such non-ideal, naturally occurring materials, the radius of curvature could vary on scale of the contact patch—particularly for the case of the crushed, unweathered aggregate. Additionally, local crushing and microcracking are likely to occur during loading in natural materials. Such permanent deformation will alter the local radius of curvature, and possibly increase the no-load contact area, both of which can substantially change the force–displacement relationship of the contact.

With the above considerations in mind, we have characterized the radius of curvature at the contact point for the grains employed in the present experiments using a readily available optical microscopy system that has sufficient resolution (better than 100 μm) to characterize our relatively large grains. Scaled, digital micrographs were obtained before and after testing, and a quantitative image processor (Image Pro Plus) was used to obtain profiles of the grains as shown in Fig. 9. The scaled outlines were subjected to a least squares analysis to determine the radius of a best-fit circular arc centered on the point of contact. The results of this analysis are given in Table 1.

For the case of the gneiss specimens, each grain pair consisted of a pointed grain impinging on a nominally flat grain, and we report the curvature only of the pointed grain. The weathered grains both appeared to be nominally spherical to the unaided eye, but were irregularly shaped when viewed under the microscope. Consequently, the curvature for those grains was determined for the lobes that were actually in contact.

We note that the reported values of curvature were obtained after testing, and are applicable to the mechanical data that are presented. The grains were intentionally selected to be robust, and there was no visible evidence of damage after testing. However, it is cautioned that the load–deformation data presented here may not be representative of virgin loading behavior. Our on-going work is addressing the matter of

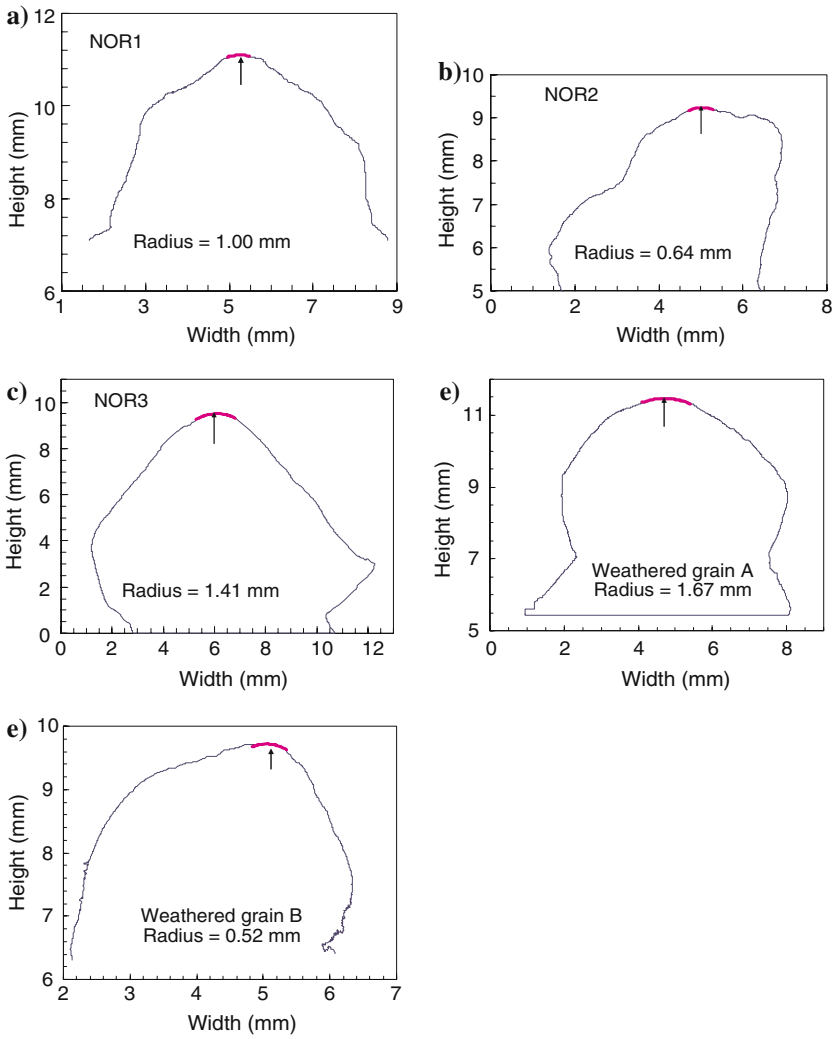

Fig. 9 Plots of the digitized outlines of the grains used in the experiments. The radius of curvature was determined by a least squares analysis as described in the text. Circular arcs have been over-plotted to indicate the regions of the outlines used in the analysis. **a** The pointed grain from pair NOR1, **b** the pointed grain from pair NOR2, **c** the pointed grain from pair NOR3, **d**, **e** the two pointed grains of weathered aggregate

Table 1 Estimated radii of curvature for the grains used in the experiments

Grain pair	Radius of curvature at contact (mm)	Remarks
NOR1	1.00	Crushed, not milled
NOR2	0.64	Crushed, not milled
NOR3	1.41	Milled
Weathered (A)	1.67	Weathered NH gravel
Weathered (B)	0.52	
Brass pins	2.32	
Nylon pins	2.23	

Only one value is reported for grain pairs NOR1–3 because they consisted of one pointed grain and one nominally flat grain. The weathered pair consisted of two pointed grains

virgin versus conditioned contact behavior and those results will appear at a later date.

7 Reference experiments

Reference experiments were conducted on specimens of commercial nylon and brass to validate the performance of the system using manufactured materials of known mechanical properties. Pairs of pins with the geometry shown in Fig. 10 were machined and the radius of curvature of the contact region on each pin was determined as described in the preceding section. These specimens were subjected to ramp loading at 1 N s^{-1} and/or haversine loading at 1 Hz over a range of peak force, and the load–displacement results are shown in Fig. 11 in log-log space. The data for the brass specimens were obtained from a ramp loading test and the nylon data were determined from a series of cyclic loading tests with increasing peak loads as indicated. Although these results exhibit a certain degree of scatter, the data cluster about a slope of 3/2, which is indicative of Hertzian behavior. Moreover, the displacements agree quantitatively with the approach distance δ calculated for elastic spheres of radius R and Young's modulus E, resulting from a normal force N (e.g., [17]):

$$\delta = 2\left[\frac{3(1-\upsilon^2)N}{4ER^{1/2}}\right]^{2/3}. \tag{3}$$

Figure 11 plots this relationship (solid lines) for the brass and nylon pins used in these experiments. The radius of curvature at the contact points of the brass and nylon pins was determined to be 2 mm using the method described in a previous section. The good agreement between the calculated and experimentally determined values for the brass in Fig. 11 requires a Young's modulus of 80 GPa, which is reasonable for this material (modulus values in the literature typically range from 90 to 125 GPa depending on composition and treatment). Since the reported values of the modulus of elasticity for nylon vary somewhat, we determined the bulk modulus of our nylon stock directly in the test apparatus and arrived at a value of 1.6 GPa. The data plotted in Fig. 11 account for the deformation of the threaded portions of the specimens. Because of the relatively low modulus of the nylon, that contribution was approximately 10% of the total. By contrast, since the modulus of brass is relatively high, the contribution from the threaded portion of the brass pins was $<1\%$ of the total deformation.

8 Experimental results

The goals of these initial experiments were to demonstrate the viability of the experimental equipment and methods, and explore several fundamental aspects of contact behavior under normal loading. We note that applied loads of $\leqslant 25$ N were in some cases sufficient to cause damage of the contact

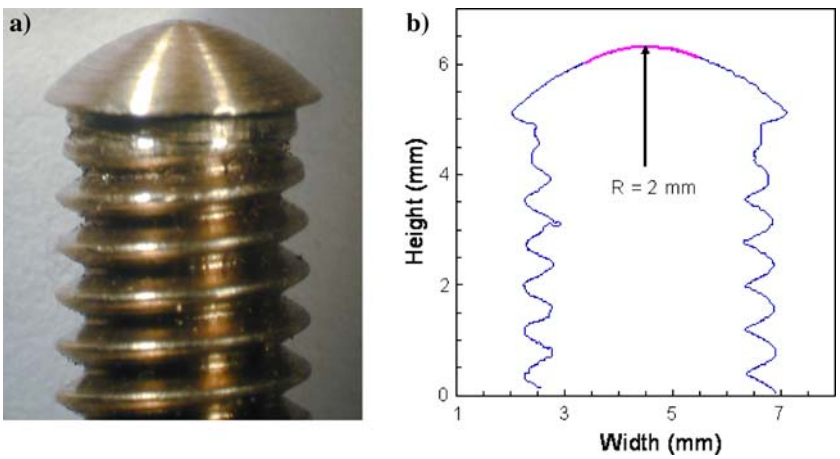

Fig. 10 Micrograph of one of the brass pins used in the reference experiments (**a**) and the outline of the pin obtained from a quantitative image processor used to determine the radius of curvature of the contact region (**b**)

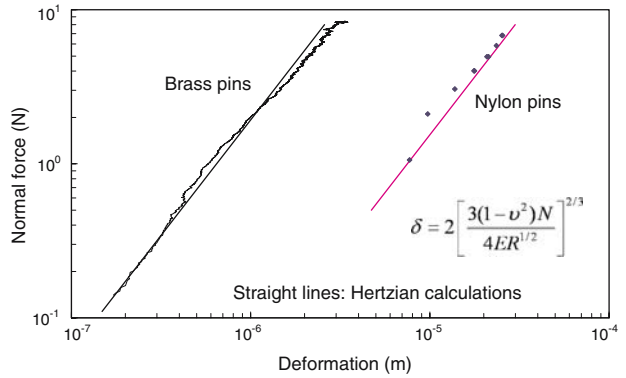

Fig. 11 Force versus displacement data from ramp and cyclic loading experiments on brass and nylon pins, and the results of a Hertzian contact calculation (*straight lines*) for each material

points, as evidenced by audible reports during load application. Although we did not employ methods to track or quantify damage in these initial experiments, this will be a point of interest in future work. Since most of the grain pairs that were examined had been subjected to extensive load cyclic during the course of the experiments, the results presented below are not expected to be representative of the virgin state of the material. A related aspect of the contact problem that will be examined in future experiments is the matter of the contact area.

The experiments reported below report briefly on monotonic or ramp loading, and then focus more closely on the cyclic loading behavior, with an emphasis on load level effects on the stiffness of the contacts.

Monotonic loading. Figure 12a shows a typical response of the weathered aggregate and the unweathered, crushed gneiss to a loading ramp. It was common for these materials to display an upward concavity to the load–deformation curve, but a logarithmic plot of these curves (see Fig. 12b) shows linear behavior at lower forces and a transition to a 3/2 power relationship at high forces.

Haversine loading. Figure 13 shows the load–deformation response of the weathered aggregate and the crushed gneiss to compressive haversine loading. The weathered aggregate clearly exhibits a lower stiffness and internal friction (as evidenced by the lower slope and much larger hysteresis loops) than the crushed gneiss, although it is noted that both of the weathered grains were nominally spherical whereas the gneiss grain pairs always consisted on one curved and one nominally flat grain. The weathered aggregate also exhibits a more significant amount of permanent deformation per load cycle. Excluding the first load cycle, the average slope of the hysteresis loops of the weathered aggregate

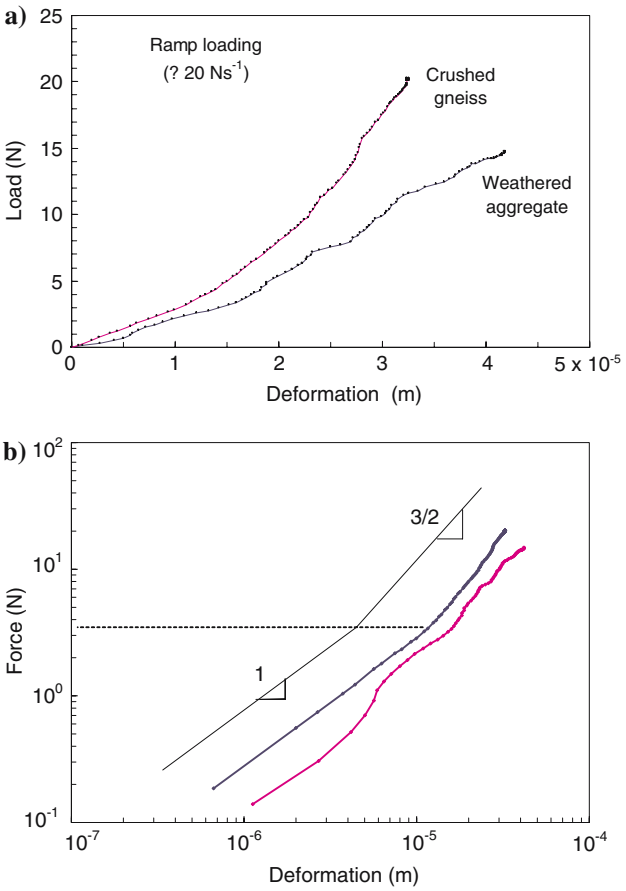

Fig. 12 Load–deformation behavior for the gneiss and weathered aggregate pairs plotted with **a** linear scales, and **b** logarithmic scales. The latter plot shows lines with slopes of 1 and 3/2 for reference. The loading rate was 20 N s^{-1}

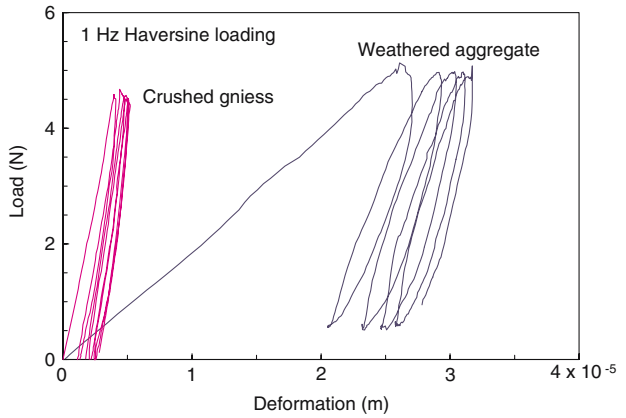

Fig. 13 Load versus deformation for the crushed gneiss and weathered aggregate pairs subjected to haversine loading

is 0.627 N μm^{-1}, and the average internal friction is 0.175. In comparison, the response of gneiss is 1.72 N μm^{-1} and 0.12, respectively for the slope and internal friction.

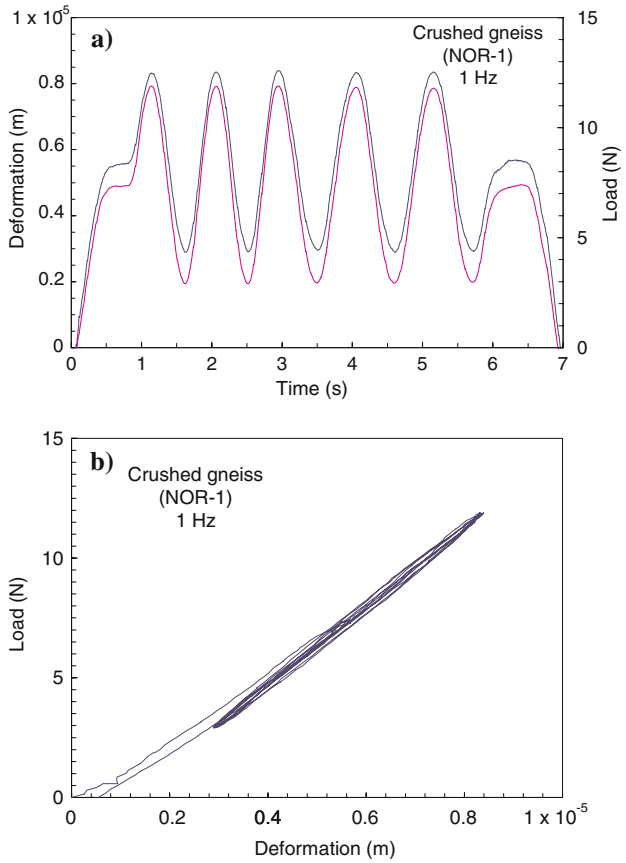

Fig. 14 Response of crushed gneiss to a ±5 N sinusoidal wave superimposed on a background force of 8 N. **a** Force and displacement versus time. **b** Load versus deformation

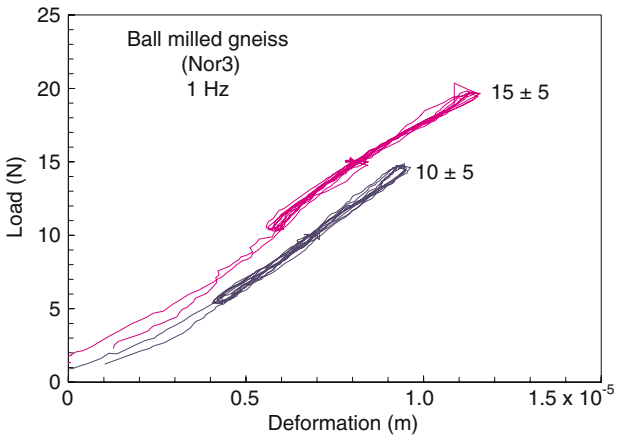

Fig. 15 Load–deformation response of ball-milled gneiss subjected to sinusoidal loading superimposed on background forces of 10 and 15 N as indicated. The cyclic loading frequency was 1 Hz

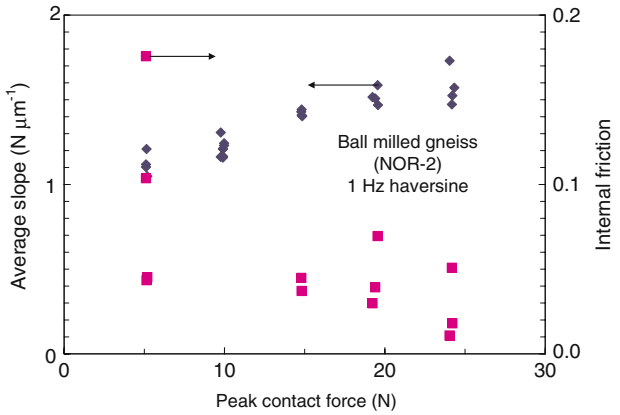

Fig. 16 Average slope of the hysteresis loops and internal friction versus peak contact force for the ball milled gneiss

Sinusoidal loading superimposed on a background load. Figure 14 illustrates the case of a sine wave superimposed on a constant background load level. The background load was applied at a rate of approximately 20 N s^{-1}, and maintained for a brief period before the sinusoidal loading was initiated. Typically 3–5 cycles of the sine wave were applied, and the background load was subsequently ramped to zero as indicated in the figure. Figure 14a shows the experiment in load-time space, and Fig. 14b shows the load–deformation behavior. The background load levels were applied in the sequence of 5, 10, 15 and 20 N, and the amplitude of the superimposed sinusoidal loading was either ±5 or ±10 N. The frequency of the sinusoidal loading was 1 Hz.

Figure 15 shows typical behavior for the gneiss for background loads of 10 and 15 N, and a superimposed cyclic load of ±5 N. Although the response of the specimens to this loading sequence was somewhat variable, the general effect of the increased background force was to decrease the internal friction observed under cyclic loading. This decrease was usually accompanied by a small increase in the slope of the load–deflection curve. Figure 16 illustrates this trend with a plot of the slope of the load–deflection curve and the internal friction versus the peak (e.g., background load + the cyclic load amplitude) load level. Although the data are somewhat sporadic in this regard, there was a tendency for the slope to increase and the internal friction to decrease with repeated cycling during each individual set of load cycles. Additionally, both quantities frequently tended toward an equilibrium value with repeated load cycling. This could be the result of attenuating damage at the contact point, and will be studied in future experiments.

Frequency effects under haversine loading. We examined the response under haversine loading for frequencies of 3×10^{-2} and 10^{-1} Hz to establish a baseline for behavior and to explore the behavior of our experimental apparatus at lower frequencies. Figure 17a shows several cycles of the force–displacement response of the gneiss to a 20 N haversine at 10^{-1} Hz. Note that the initial load-up has the upward

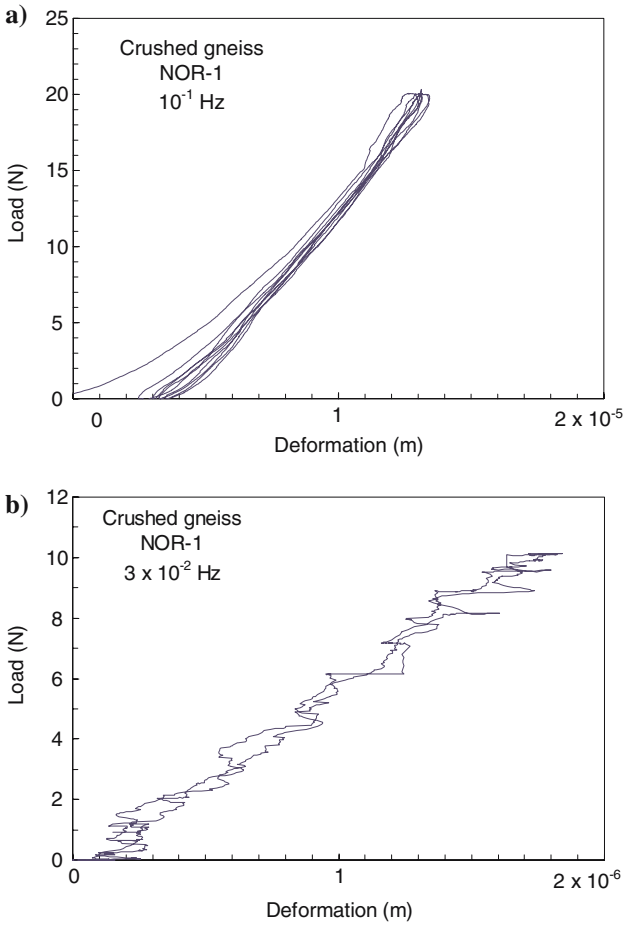

Fig. 17 Load–deformation response of the crushed gneiss to haversine loading at frequencies of **a** 10^{-1} Hz and **b** 3×10^{-2} Hz

concavity observed at the higher frequencies discussed above, and that the response reaches an apparent steady state after the first cycle. Excluding the first cycle, the average slope observed for this specimen was approximately $2\,\mathrm{N}\,\mu\mathrm{m}^{-1}$ and the internal friction was 0.04. At the somewhat lower frequency of 3×10^{-2} Hz, shown in Fig. 17b, the overall response was similar (the average slope was $2.4\,\mathrm{N}\,\mu\mathrm{m}^{-1}$), but the load–deformation plot is noticeably less smooth than the higher frequency response, possibly the result of stick–slip behavior that was not evident at the higher frequencies. Perhaps because of the contributions to the hysteresis loop area of the stick–slip behavior, a higher internal friction value of 0.12 was observed at the lower frequency.

9 Discussion

The results presented above make it clear that grain-scale experiments provide important quantitative information on particle mechanics and are sufficiently sensitive to particle characteristics to support the development of physically based relationships needed for discrete element models. Although we have presented data that we feel are representative of the behavior of the specimens under consideration, it is emphasized that we are dealing with naturally occurring material, and a certain degree of variability in the mechanical response should be expected. Additionally, the extent to which the observed behavior is influenced by the vagaries of a particular contact versus variations in the intrinsic properties of the grains is a matter of concern and will be the subject of future work. That being said, the systematic differences found in the stiffness of the test materials strongly suggest that intrinsic properties of the grains influence the mechanics of their interaction to a measurable degree. Although the data presented above are limited, they do display a number of trends that have noteworthy implications for the numerical modeling effort which are now considered.

The force–displacement curves observed during monotonic (Fig. 12) and cyclic (Fig. 17a) loading where the force varied from a nominal no-load contact to 15–20 N are macroscopically concave upward. However, as noted above, the ramp loading experiments showed linear behavior at low forces and undergo a transition to a 3/2 power law dependence at a nominal force of 3.5 N for the gneiss and possibly at a somewhat lower force for the weathered aggregate. The variability in the latter curve prevents a more precise determination of the transition force. This shift to non-linear behavior is also evident under cyclic loading, as indicated in Fig. 17a. Non-linear behavior is not clearly evident in experiments in which the force was either low (< 5 N) or varied over a relatively small range (e.g., Figs. 13, 14, and 15). It is possible that the behavior in these experiments appears to be linear primarily because the force range was too small for the relatively weak non-linearly to be observed. Nonetheless, there is some evidence of seating effects in the cyclic loading experiments since the initial loading curves are generally different from all subsequent cycles.

The upward concavity in the particle-scale load–deformation relationship suggests a relationship to the pressure sensitivity of the elastic constants often found in macro-scale experiments. This is in contrast to the alternative explanation that the increase in stiffness might be related to subtle recoverable changes in contact topology. We note that the upward concavity observed in the load–deformation behavior is not generally addressed in DEM simulations, and it will be a point of interest in future work to determine the extent to which this aspect of particle-scale behavior is reflected in the macro-scale behavior of the particulate medium. The fact that the non-linear behavior becomes evident only when the normal force varies over a relatively wide range suggests that linear force–displacement relationships may be sufficient to model grain-scale behavior for either low

absolute levels of inter-particle forces or for relatively small changes in inter-particle force.

As noted in a previous section, the force–displacement relationship can be understood in greater depth with the information gained from the experiments in which cyclic loading was superimposed on a background force. The example results from these experiments (Fig. 16) show that the elastic stiffness increases with the normal force, verifying the trend evident in the monotonic loading experiments. Additionally, it shows that the internal friction (from which the inelastic strain can be calculated) decreases as the mean normal force increases.

With a certain amount of scatter, the internal friction appears to be independent of frequency, at least over the relatively narrow range examined here, indicating that energy dissipation is by true hysteretic behavior, rather than some form of viscoelasticity. This micro-scale observation is thus consistent with observations that the constitutive response of granular media at the macro-scale is primarily rate-independent. We note that this conclusion applies to the case of small strains only, and that it will be useful to examine wider ranges of force and frequency to verify the trends seen here.

Comparing the behavior of the test materials under normal cyclic loading, we see that the weathered aggregate displayed appreciably greater hysteresis than the crushed gneiss. The reason for the higher loss in the weathered material is not apparent at this time, although the likely causes for later investigation include increased contact area, the extent to which the weathered surfaces engage each other microscopically, and possible loss mechanisms associated with defects within the grains. Regardless of its source, the substantial difference in hysteresis between the two materials is surprising, and the loss in the gneiss appears to be much less than expected based on that required to get realistic DEM simulations. Given that the internal friction increases noticeably with decreasing mean contact force, and that a variety of applications deal with forces that are substantially lower than those reported herein, it is of particular interest to explore the extent to which higher internal friction values are characteristic of contacts subjected to low forces. Consequently, we are currently working to extend the operating range of our system to considerably lower forces.

The present experiments were not equipped to quantify microcracking at the contact point. As noted above, a conscious effort was made to avoid using results from experiments where audible damage occurred, but this does not preclude damage on a very fine scale. Future work will incorporate an acoustic emissions monitoring system to provide some insight regarding the experimental conditions associated with microcracking at the contact point.

The experimental techniques described in this paper are equally applicable to bonded particles, for which micromechanical measurements are of great interest. The case of bonded particles is problematic because it is difficult to relate micro-scale behavior to emergent behavior, and macro-scale observations are less useful to identifying the mechanics of bonding forces on the scale of grains. Bonding forces can include electrostatic forces, capillary tension, and cementation. They can act in tangential, normal, and bending modes either independently or coupled through a limit surface (Fig. 5). Such complex interactions cannot be quantified from macro-scale experiments, but the grain-scale experimental methods applied here can be used to isolate and quantify the deformation and failure modes of interest. As of this writing, laboratory experiments on bonded granular media have been initiated.

Our on-going investigations that couple contact measurements with both macro-scale experiments and DEM simulations should lay the groundwork for procedures to use simulations to develop macro-scale engineering properties from micro-scale measurements. This approach is particularly attractive for lunar and planetary mission planning where opportunities to experimentally determine the in-situ engineering properties of the regoliths are limited.

10 Summary and conclusions

Equipment and methods have been developed to conduct grain-scale mechanical properties experiments on unbonded grain pairs. The results of contact experiments using processed materials (brass and nylon) were presented to validate our experimental and analytical methods. Additionally, methods were presented to determine the radius of curvature at the contact points. Example results on two types of naturally occurring materials (crushed gneiss and a weathered gravel) illustrated normal force–displacement relationships under monotonic and cycle loading conditions, and an approach to integrating such grain-scale experimental results into a discrete element modeling framework was discussed.

The experimental data provided information on the elastic stiffness and energy dissipation of contacts between particle pairs as functions of mean force level and frequency. A substantial difference was observed in elastic stiffness and the hysteretic loss of the two materials under consideration, and the implications of the latter observation were discussed in the context of discrete element model development.

Pressure sensitivity of the contact stiffness was apparent in the initial ramp loading of the contact. Both material types displayed a 3/2 power law dependence of the force–displacement behavior when the range of applied normal force was sufficiently high, and this dependency was sustained under repeated load cycling. Because of its relatively mild curvature, the force–displacement behavior appeared to be linear when the range of applied force was low (<5 N).

The initial results suggest several topics of research using the DEM. It is clearly of interest to understand the elastic response under various background force levels and this would certainly be essential to any investigation into wave propagation in granular media. The observed variation in contact response under repeated loading is highly relevant to understanding the effects of specimen formation and the relationship between reconstituted versus in-situ behavior. A related issue is "aging" of sedimented deposits, which have been observed to gain strength with the passage of time. The common feature of all these topics is the direct measurement of contact properties, which allows separation of contact behavior from structural features such as force chains and contact orientation.

Acknowledgments This work was supported by the Engineer Research and Development Center's basic research project entitled "Stress transfer in granular media". The authors express their appreciation to Chris Williams for his help in developing the electronic components of the experimental system, to John Gagnon for developing the system control and data acquisition software and help with conducting experiments, to William Burch for his contributions to the design and fabrication of the experimental hardware, to Emily Andreas for her help in conducting the experiments, and to Dr. Johannes Wibowo for simulations giving insight into the many problem of calibrating parameters for bonded media. We are also grateful for the insightful comments that were provided by two anonymous reviewers of the manuscript.

References

1. Arthur, J.F., Chua, S., Dunstan, T., Rodriguez del C.J.I.: Principal stress rotation: a missing parameter. J. Geotechn. Eng. Div. ASCE, **106**(No GT4), 419–433 (1980)
2. Carpick, R.W., Ogletree, D.F., Salmeron, M.: Lateral stiffness: a new nanomechanical measurement for the determination of shear strengths with friction force microscopy. Appl. Phys. Lett. **70**(12), 1548–1550 (1997)
3. Cole, D.M.: A model for the anelastic straining of saline ice subjected to cyclic loading. Phil. Mag. A. **72**(1), 230–239 (1995)
4. Cole, D.M.: A dislocation-based model for creep recovery in ice. Phil. Mag. **84**(30), 3217–3234 (2004)
5. Cole, D.M., Durell, G.D.: The cyclic loading of saline ice. Phil. Mag. **72**(1), 209–229 (1995)
6. Cole, D.M., Durell, G.D.: A dislocation-based analysis of strain history effects in ice. Phil. Mag. A. **81**(7), 1849–1872 (2001)
7. Cundall, P.A., Strack, O.D.L.: A discrete numerical model for granular assemblies. Geotechnique **29**(1), 47–65 (1979)
8. D'Addetta, G.A.: Discrete model for cohesive frictional materials. Ph.D. Thesis, Bericht Nr. 42, Institute für Baustatik der Universität Stuttgart, Germany (2004)
9. D'Addetta, G.A., Ramm, E.: A microstructure-based simulation environment on the basis of an interface enhanced particle model. Granul. Matter **8**, 159–174 (2006)
10. Gardiner, B.S., Tordesillas, A.: Micromechanics of shear bands. Int. J. Solids Struct. **41**(21), 5885–5901 (2004)
11. Goldenberg, C., Goldhirsch, I.: Force chains, microelasticity and macroelasticity. Phys. Rev. Lett. **89**, 084320 (2002)
12. Goldenberg, C., Goldhirsch, I.: Friction enhances elasticity in granular solids. Nature **435**, 188–191 (2005)
13. Grierson, D.S., Flater, E.E., Carpick, R.W.: Accounting for the JKR-DMT transition in adhesion and friction measurements with atomic force microscopy. J. Adhes. Sci. Technol. **19**(3–5), 291–311 (2005)
14. Horne, H.M., Deere, D.U.: Frictional characteristics of minerals. Geotechnique **12**, 319–335 (1962)
15. Kappl, M., Heim, L., Butt, H.-J., Luding, S., Tykhoniuk, R., Tomas, J.: From grains to powders: from single particle contact mechanics measurements to bulk powder properties. In: Garcia-Rojo, R., Herrmann, H.J., McNamara, S. (eds.) Powders and grains 2005, Stuttgart, July 2005, pp. 493–497. Balkema, Leiden (2005)
16. Majmudar, T.S., Behringer, R.P.: Contact force measurements and stress-induced anisotropy in granular materials. Nature **435**, 1079–1082 (2005)
17. Mindlin, R.D., Deresiewicz, H.: Elastic spheres in contact under varying oblique forces. ASME J. Appl. Mech. **20**, 327–344 (1953)
18. Nowick, A.S., Berry, B.S.: Anelastic relaxation in crystalline solids. pp. 677 Academic, New York (1972)
19. Oda, M., Kazama, H.: Microstructure of shear bands and its relation to the mechanisms of dilatancy and failure of dense granular soils. Geotechnique **48**(4), 465–481 (1998)
20. Oda, M., Konishi, J., Nemat-Nasser, S.: Experimental miomechanical evaluation of strength of granular materials: effects of particle rolling. Mech. Mater. **1**, 269–283 (1982)
21. Peters, J.F., Muthuswamy, M., Wibowo, J., Tordesillas, A.: Characterization of force chains in granular material. Phys. Rev. E. **72**(4), 041307 (2005)
22. Potyondy, D.O., Cundall, P.A.: A bonded-particle model for rock. Int. J. Rock Mech. Min. Sci. **41**, 1329–1364 (2004)
23. Tordesillas, A., Walsh, S.D.C., Gardiner, B.S.: Bridging the length scales: micromechanics of granular media. Bit Numer. Math. **44**(3), 539–556 (2000)